

**1 of 1**

**DISCLAIMER**

This report was prepared as an account of work sponsored by an agency of the United States Government. Neither the United States Government nor any agency thereof, nor any of their employees, makes any warranty, express or implied, or assumes any legal liability or responsibility for the accuracy, completeness, or usefulness of any information, apparatus, product, or process disclosed, or represents that its use would not infringe privately owned rights. Reference herein to any specific commercial product, process, or service by trade name, trademark, manufacturer, or otherwise does not necessarily constitute or imply its endorsement, recommendation, or favoring by the United States Government or any agency thereof. The views and opinions of authors expressed herein do not necessarily state or reflect those of the United States Government or any agency thereof.

**AN ANALYSIS OF MULTIPLE PARTICLE SETTLING  
FOR LMR BACKUP SHUTDOWN SYSTEMS**

BY

**RICHARD WAYNE BROCK**

**B.S., University of Illinois, 1990**

**THESIS**

**Submitted in partial fulfillment of the requirements  
for the degree of Master of Science in Nuclear Engineering  
in the Graduate College of the  
University of Illinois at Urbana-Champaign, 1992**

**Urbana, Illinois**

**MASTER**

UNIVERSITY OF ILLINOIS AT URBANA-CHAMPAIGN

THE GRADUATE COLLEGE

MAY 1992

WE HEREBY RECOMMEND THAT THE THESIS BY

RICHARD WAYNE BROCK

ENTITLED AN ANALYSIS OF MULTIPLE PARTICLE SETTLING

FOR LMR BACKUP SHUTDOWN SYSTEMS

BE ACCEPTED IN PARTIAL FULFILLMENT OF THE REQUIREMENTS FOR

THE DEGREE OF MASTER OF SCIENCE

*George H Miley*  
Director of Thesis Research

*Berkeley S. Jones*  
Head of Department

Committee on Final Examination

*George H Miley*  
Chairperson

*Megdi Raghib*

† Required for doctor's degree but not for master's.

## ABSTRACT

Backup shutdown systems proposed for future LMRs may employ discreet absorber particles to provide the negative reactivity insertion. When actuated, these systems release a dense packing of particles from an out-of-core region to settle into an in-core region. The multiple particle settling behavior is analyzed by the method of continuity waves. This method provides predictions of the dynamic response of the system including the average particle velocity and volume fraction of particles vs. time. Although hindered settling problems have been previously analyzed using continuity wave theory, this application represents an extension of the theory to conditions of unrestrained settling. Typical cases are analyzed and numerical results are calculated based on a semi-empirical drift-flux model. For 1/4-inch diameter boron-carbide particles in hot liquid sodium, the unrestrained settling problem assumes a steady-state solution when the average volume fraction of particles is 0.295 and the average particle velocity is 26.0 cm/s.

## ACKNOWLEDGEMENT

This research was performed under appointment to the Nuclear Engineering and Health Physics Fellowship Program administered by Oak Ridge Associated Universities for the U.S. Department of Energy. It has also been supported by the Rockford Technology Corporation of Vancouver, British Columbia. I am grateful to Dr. George Miley for our many hours of discussion and for his critique of the material. His advice and encouragement were instrumental in bringing this work to completion. Thanks also to Dr. Magdi Ragheb for his review and comments on the final draft. Finally, I wish to express my thankful appreciation to Dr. Barclay Jones and the staff of the Nuclear Engineering Department. Through their willing attention and cheerful assistance, they have facilitated the resolution of every problem I've encountered along the way. This supportive environment and the excellent facilities of the department were continually available to me and were frequently responsible for holding my frustration in check.

## TABLE OF CONTENTS

LIST OF TABLES.....	vi
LIST OF FIGURES.....	vii
LIST OF SYMBOLS.....	viii
I. INTRODUCTION.....	1
II. BACKGROUND.....	3
III. SINGLE PARTICLE SETTLING.....	7
A. An Exact Solution.....	7
B. Extension to Higher Reynolds Numbers.....	9
IV. TWO-PHASE, TWO-COMPONENT FLOW.....	15
A. Governing Equations.....	15
B. Effective Viscosity.....	20
C. Steady-State Solution.....	24
D. Extension to Higher Reynolds Numbers.....	26
E. Time-Dependent Solution.....	31
F. The Drift-flux Model.....	34
V. CONTINUITY WAVE METHOD.....	39
A. General.....	39
B. Continuity Wave Velocity.....	40
C. Application to Unrestrained Settling.....	45
VI. CONCLUSIONS.....	57
REFERENCES.....	63

## LIST OF TABLES

1. Empirical Correlations of Clift et. al.<sup>5</sup>  
for  $Re_T$  as a Function of  $Ar$ .....12
2. Time  $t^*$  and distance  $z^*$  required for a spherical  
particle of diameter  $d$  and density ratio  $\gamma = 2.84$   
to attain 90% of its terminal velocity during  
acceleration from rest in a quiescent liquid.....13
3. Empirical Correlations of Richardson and Zaki.<sup>19</sup>.....29
4. Numerical Results for Particles with  $n < 2.45$ .....52
5. Numerical Results for Particles with  $n > 2.45$ .....55

## LIST OF FIGURES

1. Proposed Backup Shutdown System for LMRs.....4
2. A Typical Curve of Drift-flux  
vs. Particle Fraction.....38
3. A Simplified Physical Model  
of the Unrestrained Settling Problem.....41
4. Drift-flux Curve Showing  
the Initial Settling Behavior.....47
5. A Time History of Multiple  
Particle Settling Behavior.....51
6. A Time History of Multiple Particle Settling  
when the Initial Settling Velocity is Limited  
by the Continuity Wave Velocity.....54
7. A Time History of Multiple Particle Settling  
Illustrating the Re-formation of Region B  
During the Final Stages of Settling.....56

## LIST OF SYMBOLS

- $A_r$  Archimedes number, Eq. (12).  
 $C_D$  Drag coefficient for a spherical particle in quiescent liquid of infinite extent, Eq. (6).  
 $C_{D\text{eff}}$  Effective drag coefficient experienced by a representative particle in a two-phase mixture of particles and fluid, Eq. (36).  
 $d$  Diameter of a spherical particle.  
 $D$  Diameter of a cylindrical duct in which particles and fluid flow.  
 $g$  Constant of gravitational acceleration.  
 $j$  Net volumetric flux or volumetric average velocity, Eq. (31).  
 $j_s$  Volumetric flux of particles, Eq. (57).  
 $j_f$  Volumetric flux of fluid, Eq. (57).  
 $j_{sf}$  Particle drift-flux, Eq. (59).  
 $j_{fs}$  Fluid drift-flux, Eq. (60).  
 $M_D$  Dimensionless displacement modulus, Eq. (13).  
 $n$  Empirical constant in Richardson and Zaki<sup>19</sup> correlation, see Eq. (40) and Table 3.  
 $p$  Pressure distribution.  
 $Re$  Reynolds number for a spherical particle, Eq. (2).  
 $Re_T$  Reynolds number based on  $v_t$ , Eq. (11).  
 $t$  Independent variable, time dimension.  
 $t^*$  Time required for a spherical particle to accelerate to 90% of its terminal velocity, Table 2.  
 $v_f$  Velocity of a flowing fluid or average velocity of the fluid phase.

- $v_s$  Velocity of a particle or average velocity of the particle phase.
- $v_{fs}$  Average relative velocity between fluid and particle phases, Eq. (20).
- $v_t$  Terminal velocity of a single spherical particle in a quiescent liquid of infinite extent, Eq. (10).
- $V_W$  Continuity wave velocity, Eq. (71).
- $V_S$  Shock wave velocity, Eq. (80).
- $W$  In Table 1,  $W = \log_{10} Ar$ .
- $z$  Independent variable, spatial dimension.
- $z^*$  Distance required for a spherical particle to accelerate to 90% of its terminal velocity, Table 2.
- $\alpha$  Average volume fraction of particles, Eq. (14).
- $\Delta_A$  Empirical constant, corrects added mass term for inertial effects, Eqs. (4) and (35).
- $\Delta_H$  Empirical constant, corrects Basset history term for inertial effects, Eqs. (4) and (35).
- $\gamma$  Ratio of particle density to fluid density, Eq. (7).
- $\delta$  Particle diffusivity, Eqs. (73), (74), (75) and (78).
- $\epsilon$  Average volume fraction of fluid, Eq. (15).
- $\mu$  Viscosity of a pure fluid phase.
- $\mu_{eff}$  Effective viscosity of a two-phase mixture of spherical particles and fluid, Eq. (28).
- $\rho_f$  Density of a pure fluid phase.
- $\rho_s$  Density of a particle.
- $\sigma$  Shear stress distribution at the wall of a vertical duct.
- $\tau$  Dimensionless time, Eq. (13).

## I. INTRODUCTION

Defense-in-depth is a principle which is well established in conventional Light Water Reactor (LWR) design. This principle requires the designer to provide redundant and diverse means to fulfill each major safety function. The major safety functions include containment, heat removal from the core and reactivity control. Backup systems are designed to fulfill each one of these functions so that a single malfunction in any system will not place the plant in an unsafe condition.

The reactivity control function in typical LWRs is accomplished by complementary systems consisting of mechanical control rods and boron injection. Thus, in the event of an unforeseen design flaw or accident sequence resulting in the common mode failure of all control rods, the boron injection system provides a backup method of core shutdown. Defense-in-depth is hereby achieved when redundant and diverse means for inserting absorber material into the core are provided.

In order to apply the same standard of defense-in-depth to the reactivity control systems of advanced Liquid Metal Reactor (LMR) designs, a backup method for inserting absorber material into the core must be developed. Direct injection of boron compounds into liquid metal coolants

does not seem practical due to the difficulty of chemical separation. Sliwinski<sup>1</sup> has proposed a system which would inject discrete boron particles into the core of an LWR. Although this proposal has not gained acceptance, particle injection may be a practical alternative for LMRs. Discrete boron carbide particles could be easily separated by mechanical means.

A variety of different backup shutdown systems have been proposed for LMRs. Some examples of those which employ the settling of discrete absorber particles are reviewed in Section II. The objective of this report is to determine a method for predicting the settling speed of the particles in a dense mixture. The settling speed of the particles is directly related to the negative reactivity insertion rate which drives the core to a subcritical condition. Thus, a determination of the settling speed is essential for understanding the dynamic operation of the shutdown system and for evaluating the core response.

In Section III, we review an analytic solution for the motion of a single particle which is released from rest in a quiescent liquid. For an analysis of multiple particle settling, we appeal to the semi-empirical drift-flux model as developed in Section IV. Dynamic conditions are analyzed by the method of continuity waves. The continuity wave method and some example calculations using this

methodology are given in Section V. Finally, Section VI contains a summary of conclusions.

## II. BACKGROUND

In order to provide a redundant and diverse means of shutdown in LMR cores, several systems have been suggested. Our interest is primarily focused on those systems which utilize discrete absorber particles to provide the reactivity insertion. In these systems, the absorber particles settle from an out-of-core region to an in-core region when the system is actuated. Actuation may be initiated under conditions of low flow, high temperature, over-power or some combination of these. In any case, the settling behavior of a dense mixture of discrete particles in a liquid medium is the physical process which characterizes the dynamic operation of these systems.

The illustration in Fig. 1 is one concept that the author has proposed for a backup shutdown system in LMRs.<sup>2</sup> The absorber material consists of boron carbide microspheres which are maintained in a position above the core during normal operation. A mechanical flow control damper at the bottom of the storage compartment opens when the system is actuated. When this damper opens, the absorber particles fall into the in-core region and a reactor shutdown results.

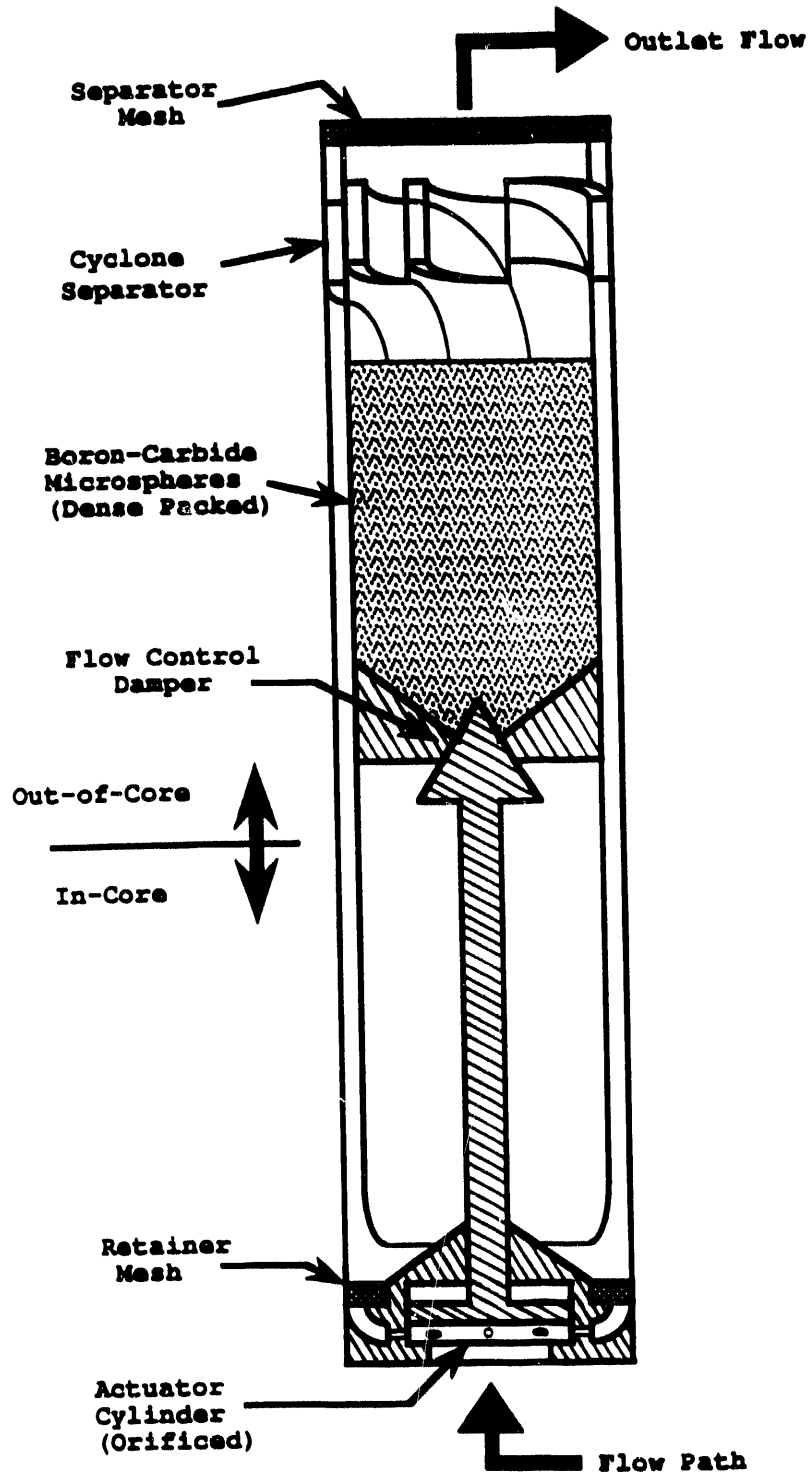


Figure 1: Proposed Backup Shutdown System for LMRs.

The flow control damper is connected to an actuating cylinder that is normally held shut by the force applied from the core inlet pressure acting on the bottom of the actuating piston. The system actuates when flow through the core drops to a point that the inlet pressure is insufficient to maintain the damper in the closed position. When core inlet pressure is restored, the damper closes and orifices in the cylinder wall are exposed. The flow of primary coolant through the orificed cylinder wall is just sufficient to transport the particles upward through the annular region. The cyclone separator at the top of the annular duct disengages the particles from the flowstream. Normal operation is restored when all of the absorber particles have been transferred from the in-core region to the out-of-core region. The device is sized so as to occupy a fuel assembly position in the core grid.

An alternative design, investigated by Specht *et. al.*<sup>3</sup> of Atomics International utilizes 1/4-inch diameter tantalum balls for the absorber material. The balls are maintained in an out-of-core region by the hydraulic drag force exerted on them by the flow of primary coolant past them. When the flow rate through the device decreases to the point that the weight of the particles can no longer be supported, the balls settle into an in-core region. Thus, actuation occurs automatically upon failure of the primary

coolant pumps. In addition, a thermally actuated flow shutoff valve with a curie-point trigger provides inherent protection for over-power transients.

As a final example, we consider the ultimate shutdown system of General Electric's advanced LMR conceptual design.<sup>4</sup> The ultimate shutdown system is designed to shutdown the reactor in the event of control rod failure after inherent reactivity feedbacks have terminated the accident transient and brought the core to a safe stable condition. The actuation sequence is therefore initiated only by operator action.

The ultimate shutdown system utilizes 1/4-inch diameter boron carbide balls as the absorber material. During normal operation, the absorber balls are stored in a canister mounted on the closure head. When the system is actuated, a diaphragm at the bottom of the storage canister is ruptured and the balls fall through a guide tube. The guide tube extends through the sodium pool and directs the balls into a catcher assembly at the center position of the core grid. Normal flow of primary coolant through the system is minimal so that actuation may occur regardless of the core inlet pressure. Normal operation is established only after the center core assembly is removed and replaced. This operation is performed with the normal fuel handling equipment.

Backup shutdown systems of the type described above could complement a system of mechanical control rods by providing a redundant and diverse shutdown mechanism in future LMRs. Those systems which actuate automatically on conditions of low flow, high temperature or over-power could enhance the operational safety by adding an element of passive safety to the design. In this type of system, the insertion of absorber material into the core is accomplished by the settling of a two-phase mixture of particles and fluid. In order to gain a perspective on the physical processes which are significant in multiple particle settling behavior, we first consider the case of single particle settling.

### III. SINGLE PARTICLE SETTLING

#### A. An Exact Solution

The equation of motion for a single spherical particle which is released from rest in a large body of stagnant fluid is:<sup>5</sup>

$$\frac{\pi d^3}{6} (\rho_s + \frac{1}{2} \rho_f) \frac{dv}{dt} = \frac{\pi d^3}{6} g (\rho_s - \rho_f) - 3\pi d \mu v - \frac{3}{2} d^2 \sqrt{\pi \mu \rho_f} \int_0^t \frac{dv}{dt'} \frac{dt'}{\sqrt{t-t'}} \quad (1)$$

Here, positive forces are defined in the downward direction. The symbols are defined as:

v = particle velocity  
 d = particle diameter  
 $\rho_s$  = particle density  
 $\rho_f$  = fluid density  
 $\mu$  = fluid viscosity  
 g = acceleration of gravity

The left-hand side of Eq. (1) represents the force required to accelerate the "apparent" mass of the particle. An "added" mass component,  $1/2(\pi/6d^3\rho_f)$  arises because acceleration of the particle requires acceleration of the surrounding fluid. The right hand side of Eq. (1) is an algebraic sum of the forces which act on the particle. These forces are: a net body force consisting of gravitational attraction minus buoyancy; a viscous drag force which is proportional to the particle velocity; and the "Basset" force which adds a dynamic component to the viscous drag force, depending on the acceleration history of the particle. This equation incorporates the Stokes drag law which arises from the "creeping" flow approximation. The validity of Eq. (1), is therefore limited to low values of the particle Reynolds number, when inertial effects can be neglected. Here, the particle Reynolds number is based on the diameter of the particle, hence:

$$Re = \frac{\rho_f dv}{\mu} \quad (2)$$

Equation (1) has a steady-state solution given by:

$$v_t = \frac{d^2 g(\rho_s - \rho_f)}{18\mu} \quad (3)$$

This is the terminal velocity of a spherical particle in a quiescent fluid. Alternatively, Eq. (3) gives the average upward fluid velocity necessary to maintain the particle suspended in a stationary position.

#### B. Extension to Higher Reynolds Numbers

Following the discussion in Clift et. al.,<sup>5</sup> Eq. (1) can be extended to higher Reynolds numbers as:

$$\frac{\pi d^3 (\rho_s + \frac{1}{2} \Delta_A \rho_f) \frac{dv}{dt}}{6} = \frac{\pi d^3 g(\rho_s - \rho_f)}{6} - \frac{\pi d^2 \rho_f C_D v^2}{8} - \frac{3}{2} \Delta_H d^2 \sqrt{\pi \mu \rho_f} \int_0^t \frac{dv}{dt'} \frac{dt'}{\sqrt{t-t'}} \quad (4)$$

This equation is not rigorously valid. The creeping flow derivation has been modified by placing dimensionless coefficients  $\Delta_A$  and  $\Delta_H$  in front of the added mass and Basset history terms, respectively. Equation (4) is thus empirical in nature and  $\Delta_A$  &  $\Delta_H$  must be determined by correlations of experimental data. The Stokes drag term is also modified from Eq. (1). For higher Reynolds numbers, the steady-state drag force is given in terms of a dimensionless drag coefficient,  $C_D$ . The drag coefficient is an empirical function of the Reynolds number and has been well determined for spherical particles.

Under steady-state conditions, Eq. (4) reduces to:

$$\frac{\pi}{6}d^3g(\rho_s - \rho_f) = \frac{\pi}{8}d^2\rho_f C_D v^2 \quad (5)$$

The drag coefficient is therefore proportional to the ratio of net gravitational forces and inertial forces:

$$C_D = \frac{4dg(\gamma-1)}{3v^2} \quad (6)$$

Here,  $\gamma$  is a density ratio defined by:

$$\gamma = \frac{\rho_s}{\rho_f} \quad (7)$$

For boron carbide ( $B_4C$ ) particles in hot liquid sodium, the density ratio is:

$$\gamma = \frac{\rho_s}{\rho_f} = \frac{2510 \frac{\text{kg}}{\text{m}^3}}{883 \frac{\text{kg}}{\text{m}^3}} = 2.84 \quad (8)$$

Many empirical correlations are available for the drag coefficient. However, at low Reynolds numbers,  $\Delta_A$  and  $\Delta_H$  converge to unity and the drag coefficient converges to Stokes law:

$$C_D = \frac{24}{Re} = \frac{24\mu}{\rho_f dv} \quad (Re < 1) \quad (9)$$

When the drag coefficient in Eq. (6) has been empirically determined, we see that the general formulation for the terminal velocity of a spherical particle is:

$$v_t = \sqrt{\frac{4dg(\gamma-1)}{3C_D}} \quad (10)$$

Substituting Eq. (9) into Eq. (10), we obtain the terminal velocity in the Stokes law range of Reynolds numbers, as shown in Eq. (3). We may therefore think of Eq. (10) as a generalization of Eq. (3). The particle Reynolds number based on terminal velocity will be designated by:

$$Re_T = \frac{\rho_f dv_t}{\mu} \quad (11)$$

In order to determine the terminal velocity of a spherical particle, we define a dimensionless Archimedes number as:

$$Ar = C_D Re^2 = \frac{4d^3 g \rho_f (\rho_s - \rho_f)}{3\mu^2} \quad (12)$$

Note that the Archimedes number is a function of the fluid and particle properties only and is independent of velocity. When the Archimedes number is used to correlate experimental measurements of the Reynolds number at terminal velocity, then  $Re_T$  can be defined as an empirical function of  $Ar$ . Clift et. al.<sup>5</sup> recommend a piecewise continuous function given by the empirical correlations in Table 1. Calculation of  $Re_T$  with adjacent correlations agree within 1% at the points of discontinuity. The terminal velocity can be found from Eq. (11) when  $Re_T$  is known.

Table 1

Empirical Correlations of Clift et. al.<sup>5</sup> for  
 $Re_T$  as a Function of  $Ar$ .  $W = \log_{10} Ar$

Range	Correlation
$Ar < 73$ $Re < 2.37$	$Re = Ar/24 - 1.7569 \times 10^{-4} Ar^2$ $+ 6.9252 \times 10^{-7} Ar^3$ $- 2.3027 \times 10^{-10} Ar^4$
$73 < Ar < 580$ $2.37 < Re < 12.2$	$\log_{10} Re = -1.7095 + 1.33438 W$ $- 0.11591 W^2$
$580 < Ar < 1.55 \times 10^7$ $12.2 < Re < 6.35 \times 10^3$	$\log_{10} Re = -1.81391 + 1.34671 W$ $- 0.12427 W^2 + 0.006344 W^3$
$1.55 \times 10^7 < Ar < 5 \times 10^{10}$ $6.35 \times 10^3 < Re < 3 \times 10^5$	$\log_{10} Re = 5.33283 - 1.21728 W$ $+ 0.19007 W^2 - 0.007005 W^3$

Just as Eq. (10) is a generalization of Eq. (3), we may also think of Eq. (4) as a generalization of Eq. (1). In order to affect this generalization, the parameters  $\Delta_A$  and  $\Delta_H$  have been empirically determined by Odar and Hamilton<sup>6</sup> from measurements of the drag force on a sphere executing simple harmonic motion in a liquid. When Eq. (4) is transformed into a dimensionless form, it can be solved by numerical integration. In order to implement this transformation, the independent variables are expressed in terms of a dimensionless time  $\tau$ , and a dimensionless

displacement modulus  $M_D$ . These variables are defined as follows:

$$\begin{aligned} r &= \frac{4\mu t}{\rho_f d^2} \\ M_D &= \frac{z}{d} \end{aligned} \quad (13)$$

Clift et. al.<sup>5</sup> give a graphical representation of the solution to Eq. (4) in dimensionless form. We note that the solution is a function of the particle density ratio  $\gamma$ , and the terminal velocity Reynolds number  $Re_T$ , as well as  $r$  and  $M_D$ . Using this solution, we can calculate the time  $t^*$  and distance  $z^*$  that are required for a particle of diameter  $d$  to attain 90% of its terminal velocity during acceleration from rest. The results of this calculation are tabulated in Table 2 for several different particle sizes.

Table 2

Time  $t^*$  and distance  $z^*$  required for a spherical particle of diameter  $d$  and density ratio  $\gamma = 2.84$  to attain 90% of its terminal velocity during acceleration from rest in a quiescent liquid.

$d$ (cm)	$d$ (in)	$Re_T$	$v_t$ (cm/s)	$r$	$M_D$	$t^*$ (s)	$z^*$ (cm)
0.150	0.059	1030	26.9	0.08	12.4	0.12	1.86
0.120	0.047	714	23.2	0.12	12.1	0.11	1.46
0.090	0.035	438	19.0	0.17	11.4	0.09	1.02
0.060	0.024	213	13.9	0.3	10.6	0.07	0.64
0.030	0.012	55.0	7.16	0.88	7.7	0.05	0.23
0.015	0.006	11.7	3.04	2.0	4.4	0.03	0.07

Equation (5) shows that, for a particle traveling at its terminal velocity, there is an equilibrium of forces in which the hydrodynamic drag force is balanced by the net weight of the particle in the fluid. Therefore, the calculations of Table 2 are estimates of the time and distance that the particle travels before this force equilibrium is established.

In a practical shutdown device, the absorber particles will be required to settle a distance of several meters. From the results of Table 2, we see that the acceleration phase of their motion is of relatively short duration and displacement. Therefore, we can generally assume that a particle attains its terminal velocity immediately after release.

Until now, we have only considered the motion of a single spherical particle, settling in an unbounded fluid medium. In a mixture of particles and fluid with finite boundaries, the equations of motion are more difficult to derive and solve. The mere presence of additional particles increases the effective density and viscosity of the mixture. The motion of each particle induces motion of the surrounding fluid and transmits forces between particles. The net effect of these complicating factors is to increase the total drag force experienced by each particle. Thus, the terminal velocity of a single particle

places an upper bound on the settling velocity of a mixture.

#### IV. TWO-PHASE, TWO-COMPONENT FLOW

##### A. Governing Equations

Consider a two-phase, two-component system consisting of a mixture of identical spherical particles dispersed in an incompressible fluid and confined to a vertical duct of constant cross-section. The average volume fraction of particles, designated  $\alpha$ , will be defined as:

$$\alpha = \frac{\text{Volume of particles in a given control volume.}}{\text{Total volume of the control volume.}} \quad (14)$$

We will also define an average void fraction or average volume fraction of fluid as  $\epsilon$ :

$$\epsilon = 1 - \alpha \quad (15)$$

When these parameters are associated with a particular point in space and time, we will understand that the values are averages for a suitably sized differential volume element located at that particular point. According to Rumpf,<sup>7</sup> if a large number of particles are loosely packed in a duct with a diameter much greater than the particle diameter, a maximum particle fraction of  $\alpha \approx 0.58$  will result.

For a two-phase mixture which flows parallel to the axis of a vertical duct, the one-dimensional momentum equation is:

$$(1 - \alpha)\rho_f \left[ \frac{\partial v_f}{\partial t} + v_f \frac{\partial v_f}{\partial z} \right] + \alpha\rho_s \left[ \frac{\partial v_s}{\partial t} + v_s \frac{\partial v_s}{\partial z} \right] - g \left[ (1 - \alpha)\rho_f + \alpha\rho_s \right] - \frac{\partial p}{\partial z} - \frac{\partial \sigma}{\partial z} \quad (16)$$

Here,  $v_f$  and  $v_s$  are the velocities of the fluid and solid phases, respectively. These are defined as positive in the upward direction. Also,  $\partial p/\partial z$  is the pressure gradient and  $\partial \sigma/\partial z$  is the shear stress gradient due to friction at the wall of the duct. If the diameter of the duct  $D$ , is much larger than the particle diameter  $d$ , i.e.  $D \gg d$ ; then friction at the wall becomes negligible in comparison to the other forces, i.e.  $\sigma = 0$ .

In addition to the momentum balance of Eq. (16), the two-phase mixture must also satisfy separate mass conservation relations for each distinct phase. Since no mass transfer occurs, we obtain the following continuity equations:

$$\frac{\partial}{\partial t}(\alpha\rho_s) + \frac{\partial}{\partial z}(\alpha\rho_s v_s) = 0 \quad (17)$$

$$\frac{\partial}{\partial t}[(1 - \alpha)\rho_f] + \frac{\partial}{\partial z}[(1 - \alpha)\rho_f v_f] = 0 \quad (18)$$

Note that  $\rho_s$  and  $\rho_f$  are the material densities of the solid and fluid phases, respectively. They are therefore

constants, and may be taken outside of the differential operators.

Even with the assumption of  $\sigma = 0$ , Eqs. (16), (17) and (18) are still insufficient to determine the flow. There are four unknowns, namely:  $p$ ,  $v_g$ ,  $v_f$ , and  $\alpha$ . Hence, we need a fourth equation in order to complete the set. As discussed by Soo<sup>8</sup>, the remaining equation must account for the nature of the interface between the two phases. In this particular case, we assume that the particles are fully dispersed in the fluid with an average volume fraction of  $\alpha$ . Soo's method (see Ref. 8) calls for writing an inter-phase momentum balance equation which will account for the exchange of momentum between the phases at their mutual boundaries. Instead, we will adopt the approach taken by Zuber<sup>9</sup> as an alternative to the formalism of Soo's method. Although this form of the closure relation will differ from the form obtained by Soo, it can still account for the fundamental nature of fluid-particle and particle-particle interactions. In addition, Zuber's approach has the advantage that the closure relation is easier to derive.

In Ref. 9, Zuber builds upon the work of other investigators to write an equation which describes the motion of a single "representative" particle in a two-phase

mixture of particles and fluid. The equation of motion for a representative particle is:

$$\begin{aligned} \frac{\pi d^3 \rho_s}{6} \frac{dv_s}{dt} = & 3\pi d \mu_{eff} v_{fs} - \frac{\pi d^3 \rho_s g}{6} - \frac{\pi d^3 \partial p}{6 \partial z} - \frac{1}{2} \left[ \frac{\pi d^3 \rho_f}{6} \right] \left[ \frac{1 + 2\alpha}{1 - \alpha} \right] \frac{dv_{fs}}{dt} \\ & + \frac{3}{2} d^2 \sqrt{\pi \mu_{eff} \rho_f} \int_0^t \frac{dv_{fs}}{dt'} \frac{dt'}{\sqrt{t - t'}} \end{aligned} \quad (19)$$

Note that this equation is similar in form to Eq. (1) except that the velocity dependent forces are now functions of  $v_{fs}$ , the relative velocity between the particles and the fluid.

$$v_{fs} = v_f - v_s \quad (20)$$

In some literature,  $v_{fs}$  is referred to as the slip velocity. The sign changes between Eq. (1) and Eq. (19) are a result of reversing the direction of the positive z-axis. In Eq. (19), positive forces are defined in the upward direction.

The left-hand side of Eq. (19) is the force required to accelerate a representative particle. The right-hand side is an algebraic sum of the forces acting on the particle. The forces acting on a representative particle are: a viscous drag force; the particle weight; a force due to the hydrostatic pressure gradient; a force required to accelerate the added mass of the particle; and the Basset force which adds a dynamic component to the viscous

drag force. Since the viscous drag force is described by the Stokes drag law, Eq. (19) is rigorously valid only in the creeping flow approximation when inertial effects are negligible, *i.e.*  $Re_T < 1$ . Also note that in Eq. (19), the viscous drag force is proportional to  $\mu_{eff}$ , the effective viscosity of the two-phase mixture. The effective viscosity appears under the radical in the Basset history term as well. Finally, the added mass term in Eq. (19) includes a correction factor to account for the particle concentration in the mixture. Additional details of the derivation can be found in Ref. 9.

Earlier, it was asserted that the derivation of Eq. (19) is equivalent to Soo's procedure for obtaining a closure relation, in that the fundamental nature of fluid-particle and particle-particle interactions can be accounted for. We note that the particle concentration is explicitly accounted for in the added mass term. In addition, particle concentration effects can enter Eq. (19) through the, as yet unspecified, pressure gradient. Also, fluid-particle interactions which are velocity dependent appear as functions of the relative velocity. Finally, particle concentration as well as collision effects are implicitly included by use of the effective viscosity of the mixture.

When the effective viscosity is specified, Eq. (19) together with Eqs. (16), (17) and (18) form a complete set. In principle at least, these four equations can be solved to fully determine the functions:  $p(z,t)$ ;  $v_g(z,t)$ ;  $v_f(z,t)$ ; and  $\alpha(z,t)$ . In making this statement, we have again assumed that  $\sigma = 0$  in Eq. (16).

### B. Effective Viscosity

A number of investigators have studied the effective viscosity of two-phase mixtures which consist of solid particles suspended in a fluid medium. It is well known that the effective viscosity of the mixture is greater than the viscosity of the fluid without the presence of the particles. The earliest result was derived by Einstein<sup>10</sup> from theoretical considerations. Einstein distinguished three types of motion which a fluid element can experience. These motions are translation, rotation and dilation. A rigid particle, embedded in the fluid element does not affect the translational or rotational motion of the element. The effect on viscosity is a result of the inability of the rigid particle to experience dilational motion in the same manner as does the continuous fluid phase. In Ref. 9, Zuber offers this explanation:

The effect of the presence of particles arises because of the inability of the particle

to take part in the deformation of the flow field induced by the motion of a single particle. Since at the boundary of each solid particle the velocity of the fluid is zero, each particle contributes to the distortion of the field and thereby influences the motion, of the representative particle. This influence, i.e. resistance to motion, appears to the representative particle as a change in the viscosity which becomes a function of the concentration.

Einstein's result for the effective viscosity of a mixture is:

$$\mu_{\text{eff}} = \mu (1 + 2.5\alpha) \quad (21)$$

Here,  $\mu$  is the viscosity of the pure liquid and the constant 2.5 is a shape factor which is valid only for rigid spheres. Because this result is based on the assumption of non-interacting particles, it is restricted to low particle concentrations, i.e.  $\alpha < 0.05$ .

After Einstein's analysis of effective viscosity, several investigators have attempted to extend the theory to high particle concentrations. In addition to the shape factor for spherical particles, Mooney's<sup>11</sup> theory introduces a self-crowding factor. His result is:

$$\mu_{\text{eff}} = \mu \exp\left(\frac{2.5\alpha}{1 - k\alpha}\right) \quad (22)$$

The value of the self-crowding factor is predicted to be in the range of  $1.35 < k < 1.91$ . The best value is to be empirically determined.

Vand<sup>12</sup> developed a theory of effective viscosity for dense particle concentrations by explicitly accounting for two-particle collisions. Vand's result is:

$$\mu_{eff} = \mu \exp\left(\frac{k_1\alpha + r(k_2 - k_1)\alpha^2}{1 - Q\alpha}\right) \quad (23)$$

The significance of the constants and their theoretical values are:

$$\begin{aligned} k_1 &= 2.5 \text{ shape factor} \\ k_2 &= 3.175 \text{ collision factor} \\ r &= 4 \text{ collision time constant} \\ Q &= \frac{39}{64} \text{ hydrodynamic interaction constant} \end{aligned}$$

The theory was experimentally tested by Vand.<sup>13</sup> He found that empirically determined values of the constants agreed with the theoretical values within an experimental margin of error.

Brinkman<sup>14</sup> also developed a theory of effective viscosity for dense particle concentrations by considering the flow field around a spherical particle embedded in a porous mass. He found that:

$$\mu_{eff} = \mu \frac{(1 - \alpha)^2}{\left[1 + \frac{3}{4}\alpha\left(1 - \sqrt{\frac{8}{\alpha} - 3}\right)\right]} \quad (24)$$

Since the theory models the particles as a porous mass, it does not account for their mobility. The permeability of the porous mass is obviously related to the void fraction. However, failure to consider the relative motions of the particles which constitute the porous mass probably limits

the validity of Brinkman's result. This consideration may also be responsible for the unique form of Eq. (24).

Many empirical determinations have also appeared to predict the effective viscosity. These methods yield little insight into the physical processes which affect viscosity and the results are not generally applicable to mixtures other than those considered in the derivation. Consequently, the results may appear quite different. Carman's<sup>15</sup> result is based on flow through packings of sand and powders. He found that:

$$\mu_{eff} = \mu \frac{10a}{1-a} \quad (25)$$

Steinour<sup>16</sup> studied sedimentation of tapioca particles in oil and glass particles in water. His result is:

$$\mu_{eff} = \mu \exp(4.19a) \quad (26)$$

Oliver's<sup>17</sup> result, which is based on the data of Steinour and others, is:

$$\mu_{eff} = \mu \frac{(1-a)^2}{(1-0.75a^{0.333})(1-2.15a)} \quad (27)$$

The empirical results have obvious limitations. However, the theoretical models for effective viscosity are also of limited value. They are not generally valid in the turbulent regime because the derivations are based on viscous flow and neglect inertial effects. We do know that

there is a functional dependence on the particle fraction which can be expressed by the following relation:

$$\mu_{\text{eff}} = \frac{\mu}{f(\alpha)} \quad (28)$$

In the subsequent discussion, Eq. (28) will be used to define the effective viscosity. The specific form of the function  $f(\alpha)$  can be found from the most appropriate model for the effective viscosity.

### C. Steady-State Solution

With the effective viscosity given by Eq. (28), we are in a position to seek a solution to the governing equations found earlier. Assume first, that the ratio of particle diameter  $d$ , to the diameter of the duct  $D$ , is small. With this assumption, we let  $\sigma = 0$  in Eq. (16). Equations (16), (17), (18) and (19) now have a deterministic solution. We will first consider steady-state solutions.

For steady-state, Eq. (16) reduces to the hydrostatic pressure gradient of the mixture:

$$\frac{dp}{dz} = -g[(1 - \alpha)\rho_f + \alpha\rho_s] \quad (29)$$

Here, we see that the hydrostatic pressure gradient is simply the product of the effective density of the mixture and the constant of gravitational acceleration. The negative sign indicates that the pressure gradient is directed downward.

The  $\partial a / \partial t$  term can be eliminated from Eqs. (17) and (18) to obtain:

$$\frac{d}{dz} [(1 - \alpha)v_z + \alpha v_s] = 0 \quad (30)$$

Integration of Eq. (30), results in:

$$(1 - \alpha)v_z + \alpha v_s = j \quad (31)$$

Here, "j" is the constant of integration. We see from Eq. (31) that j can be interpreted as the volumetric average velocity. Alternatively, j can also be interpreted as the net volumetric flux.

Finally, for steady-state, Eq. (19) reduces to:

$$3\pi d \mu_{eff} v_{zs} = \frac{\pi d^3}{8} \left[ \rho_s g + \frac{dp}{dz} \right] \quad (32)$$

When the right-hand sides of Eqs. (28) and (29) are substituted into Eq. (32), we obtain:

$$3\pi d \frac{\mu}{f(\alpha)} v_{zs} = \frac{\pi d^3}{8} g \left[ \rho_s - (1 - \alpha)\rho_t - \alpha\rho_s \right]$$

$$v_{zs} = \frac{d^2 g (\rho_s - \rho_t)}{18\mu} (1 - \alpha) f(\alpha) \quad (33)$$

In view of Eq. (3), we may re-write Eq. (33) as:

$$v_{zs} = v_t (1 - \alpha) f(\alpha) \quad (34)$$

Therefore, in laminar flow, the net volumetric flux is given by Eq. (31) and the relative velocity is given by Eq. (34). We will now extend these results to higher Reynolds number flows.

#### D. Extension to Higher Reynolds Numbers

In the transition region between laminar and turbulent flow, viscous effects become less significant for increasing Reynolds numbers and inertial effects become dominant. According to Stokes law, the drag force on a spherical particle is only due to skin friction. However, skin friction becomes negligible in turbulent flow where form drag predominates. Form drag develops as a result of the pressure differential across the particle. In a two-phase mixture of particles and fluid, we expect the effective drag force experienced by each individual particle to behave in this same characteristic manner. That is, viscous effects become less significant as the Reynolds number of the particle increases. Joseph et. al.<sup>18</sup> have shown that in the turbulent regime, interactions between particles are dominated by inertial effects. We are therefore led to express the effective drag force which acts on a representative particle in terms of an effective drag coefficient,  $C_{D\text{eff}}$ . By introducing this modification into Eq. (19), we obtain:

$$\begin{aligned} \frac{\pi d^3 \rho_s}{6} \frac{dv_s}{dt} - \frac{\pi d^2 \rho_f C_{D\text{eff}} v_{ts}^2}{8} - \frac{\pi d^3 \rho_s g}{6} - \frac{\pi d^3 \delta p}{6 \delta z} - \frac{1}{2} \Delta_\lambda \left[ \frac{\pi d^3 \rho_f}{6} \right] \left[ \frac{1 + 2\alpha}{1 - \alpha} \right] \frac{dv_{ts}}{dt} \\ + \frac{3}{2} \Delta_\lambda d^2 \sqrt{\frac{\pi \mu_{\text{eff}} \rho_f}{\epsilon}} \int_0^t \frac{dv_{ts}}{dt'} \frac{dt'}{\sqrt{\epsilon - \epsilon'}} \end{aligned} \quad (35)$$

Note that Eq. (35) includes the empirical constants  $\Delta_A$  and  $\Delta_H$  which were introduced in Eq. (4). These constants modify the added mass and Basset history terms to correct for the effects of turbulence.

When  $C_{D\text{eff}}$  is specified, then the governing equations for the flow of the two-phase mixture, including inertial effects, are Eq. (35) together with Eqs. (16), (17) and (18). We will assume that the effective drag coefficient for a mixture of particles can be expressed as the product of the drag coefficient for a single particle and an unknown concentration factor. In equation form, this assumption can be stated as:

$$C_{D\text{eff}} = \frac{C_D}{g(\alpha)} \quad (36)$$

As we have already seen, Eq. (16) reduces to the hydrostatic pressure gradient of the mixture at steady-state, i.e. Eq. (29). Also, Eqs. (17) and (18) combine to yield Eq. (31). The steady-state form of Eq. (35) is:

$$\frac{\pi}{8} d^2 \rho_f C_{D\text{eff}} v_{ts}^2 = \frac{\pi}{8} d^3 \left[ \rho_s g + \frac{dp}{dz} \right] \quad (37)$$

Now, by substituting the right-hand sides of Eqs. (29) and (36) into Eq. (37), we obtain:

$$\frac{\pi}{8} d^2 \rho_f \frac{C_D}{g(\alpha)} v_{ts}^2 = \frac{\pi}{8} d^3 g \left[ \rho_s + (1 - \alpha) \rho_f + \alpha \rho_s \right]$$

$$v_{ts} = \sqrt{\frac{4dg(\gamma-1)}{3C_D}} \sqrt{(1 - \alpha)g(\alpha)} \quad (38)$$

With the general form of the particle terminal velocity defined by Eq. (10), we may express the relative velocity in Eq. (38) as:

$$v_{r0} = v_t \sqrt{(1 - \alpha)g(\alpha)} \quad (39)$$

We will think of Eq. (39) as a generalization of Eq. (34) to the turbulent flow regime. However, the function  $g(\alpha)$  must be specified if this formulation is to have any practical value.

From the analysis of a variety of experimental data, Richardson and Zaki<sup>19</sup> have found that the relative velocity can be accurately predicted by the following equation:

$$v_{r0} = v_t (1 - \alpha)^{n-1} \quad (40)$$

In this equation, the exponent "n" is a function of the terminal velocity Reynolds number and the ratio of the particle diameter to the duct diameter.

$$n = n\left(\text{Re}_T, \frac{d}{D}\right) \quad (41)$$

The empirical correlations for n are given in Table 3. The ratio  $d/D$  provides a correction for friction at the wall of the duct. Note that this correction becomes negligible for even moderately turbulent flows, i.e.  $\text{Re}_T > 200$ . We also see that n is a function of  $\text{Re}_T$  only in the transition region,  $0.2 < \text{Re}_T < 500$ . This result is consistent with the dimensional analysis of Richardson and Zaki<sup>19</sup> which

predicts that the ratio  $v_{fs}/v_t$  should be independent of  $Re_T$  whenever either viscous or inertial effects can be ignored.

Table 3

Empirical Correlations of Richardson and Zaki.<sup>19</sup>

$Re_T$	$n$
$Re_T < 0.2$	$4.65 + 19.5(d/D)$
$0.2 < Re_T < 1$	$(4.35 + 17.5(d/D)) Re_T^{-0.03}$
$1 < Re_T < 200$	$(4.45 + 18(d/D)) Re_T^{-0.1}$
$200 < Re_T < 500$	$4.45 Re_T^{-0.1}$
$Re_T > 500$	2.39

The empirical correlations of Richardson and Zaki were later verified for the lowest ranges of Reynolds numbers by the experimental data of Richardson and Meikle.<sup>20</sup> In their own experiments, Garside and Al-Dibouni<sup>21</sup> obtained a result similar to that of Richardson and Zaki, but they found that the best value of the exponent  $n$  was predicted by the following correlation:

$$n = \frac{5.09 + 0.284 Re_T^{0.877}}{1 + 0.104 Re_T^{0.877}} \quad (42)$$

In this result, we see that  $n$  approaches 5.09 for small Reynolds numbers and 2.73 for large Reynolds numbers. These values are somewhat higher than those predicted by Richardson and Zaki's correlation. This difference may be

partially accounted for by the lack of an explicit correction factor for wall friction. Similar results have also been obtained by Maude and Whitmore.<sup>22</sup> They obtained a graphical representation of  $n$  as a function of  $Re_T$ , but no equations are provided. Again, no wall correction factor is given, but their graph indicates that  $n = 4.65$  for  $Re_T < 0.1$  and  $n = 2.39$  for  $Re_T > 3000$ . Finally, Andersson<sup>23</sup> derived a semi-empirical equation for  $v_{fs}/v_t$  which is an extremely complicated function of  $\alpha$ . Equation (40) provides a form which is much more convenient to use. The correlations of some additional investigators are tabulated in Ref. 24.

By comparing Eqs. (39) and (40), we find that:

$$g(\alpha) = (1 - \alpha)^{2n-3} \quad (43)$$

Introducing this result into Eq. (36), we obtain the effective drag coefficient which is experienced by a representative particle in a two-phase mixture of particles and fluid.

$$C_{D\text{eff}} = C_D (1 - \alpha)^{3-2n} \quad (44)$$

In Eq. (44),  $C_D$  is the drag coefficient for a single particle in a pure fluid. Also, by comparison of Eqs. (34) and (39), we find that:

$$f(\alpha) = \sqrt{\frac{g(\alpha)}{1 - \alpha}} \quad (45)$$

After substitution of Eq. (43) into the above, we obtain:

$$f(\alpha) = (1 - \alpha)^{n-2} \quad (46)$$

Therefore, for small Reynolds numbers, the correlations of Richardson and Zaki give the following expression for the effective viscosity:

$$\mu_{eff} = \mu (1 - \alpha)^{-(2.65 + 19.5 \frac{d}{D})} \quad (47)$$

Note that these results are obtained from a steady-state analysis. The time-dependent solution will be considered next.

#### E. Time-Dependent Solution

We have obtained a set of governing equations for a two-phase mixture flowing through a vertical duct. This set consists of Eqs. (16), (17), (18) and (35). Equation (35) incorporates empirical factors which correct for inertial effects. These equations are therefore valid for both laminar and turbulent flow regimes. In the following discussion, we will attempt to find a time-dependent solution.

We begin with Eq. (16). When  $\sigma = 0$ , we obtain the following expression for the pressure gradient:

$$-\frac{\partial p}{\partial z} = (1 - \alpha)\rho_f \left[ \frac{\partial v_f}{\partial t} + v_f \frac{\partial v_f}{\partial z} \right] + \alpha\rho_s \left[ \frac{\partial v_s}{\partial t} + v_s \frac{\partial v_s}{\partial z} \right] + g \left[ (1 - \alpha)\rho_f + \alpha\rho_s \right] \quad (48)$$

From Eqs. (17) and (18), we have already obtained Eq. (31) for the volumetric average velocity. We arbitrarily choose to eliminate  $v_f$  in favor of  $v_s$  in the remaining equations. From Eq. (31) we find:

$$v_f = \frac{j - \alpha v_s}{1 - \alpha} \quad (49)$$

In order to provide some simplification in the remaining analysis, we will drop the added mass and Basset history terms from Eq. (35). With this simplification, we re-write Eq. (35) as:

$$\rho_s \left[ \frac{\partial v_s}{\partial t} + v_s \frac{\partial v_s}{\partial z} \right] = \frac{3\rho_f}{4d} C_{D,eff} v_s^2 - \rho_s g - \frac{\partial p}{\partial z} \quad (50)$$

Now, substituting in the pressure gradient from Eq. (48):

$$\begin{aligned} \rho_s \left[ \frac{\partial v_s}{\partial t} + v_s \frac{\partial v_s}{\partial z} \right] &= \frac{3\rho_f}{4d} C_{D,eff} v_s^2 - \rho_s g + (1 - \alpha) \rho_f \left[ \frac{\partial v_f}{\partial t} + v_f \frac{\partial v_f}{\partial z} \right] \\ &+ \alpha \rho_s \left[ \frac{\partial v_s}{\partial t} + v_s \frac{\partial v_s}{\partial z} \right] + g \left[ (1 - \alpha) \rho_f + \alpha \rho_s \right] \end{aligned} \quad (51)$$

Dividing this expression by  $\rho_f$  and rearranging we get:

$$\begin{aligned} (1 - \alpha) \gamma \left[ \frac{\partial v_s}{\partial t} + v_s \frac{\partial v_s}{\partial z} \right] &= \frac{3}{4d} C_{D,eff} v_s^2 + (1 - \alpha) \left[ \frac{\partial v_f}{\partial t} + v_f \frac{\partial v_f}{\partial z} \right] \\ &- g(1 - \alpha)(\gamma - 1) \end{aligned} \quad (52)$$

Finally, we substitute in the right-hand side of Eq. (49) to eliminate  $v_f$  and simplify the result.

$$\begin{aligned}
 (1 - \alpha)^2 \left[ \alpha + (1 - \alpha)\gamma \right] \frac{\partial v_s}{\partial t} + (1 - \alpha) \left\{ [(1 - \alpha)^2 \gamma - \alpha] v_s + \alpha^2 j \right\} \frac{\partial v_s}{\partial z} \\
 + (1 - \alpha)(v_s - j) \frac{\partial \alpha}{\partial t} - \left[ \alpha v_s^2 - (1 - \alpha)j v_s + j^2 \right] \frac{\partial \alpha}{\partial z} \\
 - \frac{3}{4d} C_{D_{eff}} (v_s^2 - 2j v_s) = \frac{3}{4d} C_{D_{eff}} j^2 - g(1 - \alpha)^3 (\gamma - 1)
 \end{aligned} \tag{53}$$

We also have, from Eq. (17):

$$\frac{\partial \alpha}{\partial t} + v_s \frac{\partial \alpha}{\partial z} + \alpha \frac{\partial v_s}{\partial z} = 0 \tag{54}$$

Equations (53) and (54) are two coupled Partial Differential Equations (PDEs) which are satisfied by the functions  $v_s(z, t)$  and  $\alpha(z, t)$ . However, the solutions cannot be obtained by exact analytical methods. Some further simplification may be obtained if physical constraints are considered. For instance, we could specify  $j = 0$  for a closed system of sedimenting particles. This constraint results from the observation that a fixed volume of settling particles displaces an equal volume of fluid at every point in the flow. Even with this simplification, a solution cannot be obtained analytically. The complexity of Eq. (53) would only increase if the added mass and Basset history terms from Eq. (35) were included.

Our efforts to find an explicit solution in the form  $v_s = v_s(z, t)$  and  $\alpha = \alpha(z, t)$ , have so far been frustrated.

However, further consideration of the continuity equation and its consequences will provide a method for predicting the dynamic behavior of a general two-phase system. This discussion will be taken up in Section V. First, it will be convenient to express the steady-state solution in terms of the drift-flux model.

#### F. The Drift-flux Model

In Section IV.C, we found that for two-phase flow, the relative velocity between the phases is given by Eq. (39). Substituting Eq. (43) into Eq. (39), we obtain:

$$v_{fs} = v_t (1 - \alpha)^{n-1} \quad (55)$$

This result was obtained empirically by Richardson and Zaki.<sup>19</sup> Recall that  $n$  is an empirical function of  $Re_T$  and  $d/D$ , (see Table 3). Note that  $Re_T$  and  $d/D$  are independent of the flow. Since  $v_t$  is also a unique function of  $Re_T$ , we may regard  $Re_T$  and  $d/D$  as parameters. Therefore the functional relationship expressed by Eq. (55) may be written as:

$$v_{fs} = F(Re_T, \frac{d}{D}; \alpha) \quad (56)$$

In other words, the relative velocity depends on the particle fraction only, without regard to the direction of the flow or the direction in which either component is flowing. Lapidus and Elgin<sup>25</sup> were the first to recognize

the significance of this result. They showed, on the basis of a theoretical argument that: "The particle knows the movement of only the fluid and not the walls and does not know whether it is moving relative to the latter or not." The relative velocity may therefore be considered as an invariant parameter of the flow. The relationship of Eq. (55) may be obtained from the results of either sedimentation or fluidization experiments. Also, fluidization experiments may involve either co-current or counter-current flow. Lapidus, Elgin and their co-workers have verified this relationship for particle-fluid systems and for gas-liquid systems, (see Refs. 22, 26, 27 and 28).

In a general two-phase flow system, the volumetric flux of each component is the volume of that component which flows across a unit cross-sectional area, per unit time. The component volumetric fluxes have the same units as velocity and are related to the component velocities as follows:

$$\begin{aligned} j_s &= \alpha v_s \\ j_f &= (1 - \alpha)v_f \end{aligned} \tag{57}$$

In some literature, the component volumetric fluxes are referred to as superficial velocities. The net volumetric flux is the sum of the component fluxes.

$$j = j_s + j_f = \alpha v_s + (1 - \alpha)v_f \tag{58}$$

The net volumetric flux is the same as the volumetric average velocity as described in the discussion following Eq. (31). The net volumetric flux is also a constant of the flow for a general two-phase system in which incompressibility of the components is assumed. This fact follows directly from continuity considerations. We have already seen, that for sedimenting particles in a closed system, the net volumetric flux is identically zero at every point in the flow. In a constant-flow fluidized system, the net volumetric flux is fixed by the volumetric flow rate of the fluid. Again,  $j$  is constant at every point in the flow.

We now want to describe the relative motion between the phases in terms of the drift-flux model. The drift-flux is defined as the volumetric flux of a component relative to a surface which is moving at the volumetric average velocity. The drift-flux of the particle phase is given by:

$$j_{s,r} = \alpha(v_s - j) = j_s - \alpha(j_s + j_r) = (1 - \alpha)j_s - \alpha j_r \quad (59)$$

Note that the drift-flux of the fluid phase is the same magnitude of, but in the opposite direction to the particle drift-flux.

$$j_{r,s} = \alpha j_r - (1 - \alpha)j_s = -j_{s,r} \quad (60)$$

In order to obtain a relationship between the drift-fluxes and the relative velocity, we substitute the definitions of the component fluxes given by Eq. (57) into Eq. (60).

$$j_{fs} = \alpha(1 - \alpha)v_f - (1 - \alpha)\alpha v_s = \alpha(1 - \alpha)v_{fs} \quad (61)$$

In view of Eq. (55), the drift-flux can be expressed as:

$$j_{fs} = -j_{sf} = \alpha(1 - \alpha)^n v_t \quad (62)$$

Here, we see that the drift-flux is another invariant parameter for a general two-phase system.

Equation (62) will be regarded as the semi-empirical drift-flux model. This model can be used to describe the interaction between the particle and fluid phases in a general two-phase flow system. Figure 2 illustrates a typical graph of the form obtained from this model. The graph of drift-flux vs. particle fraction represents the locus of all points of hydrodynamic equilibrium between the particle phase and the fluid phase. The drift-flux is maximal when the derivative of Eq. (62) vanishes. This occurs at a particle fraction of:

$$\alpha = \frac{1}{n + 1} \quad (63)$$

We see that the drift-flux attains a maximum value of:

$$(j_{fs})_{\max} = \frac{n^n}{(n + 1)^{n+1}} v_t \quad (64)$$

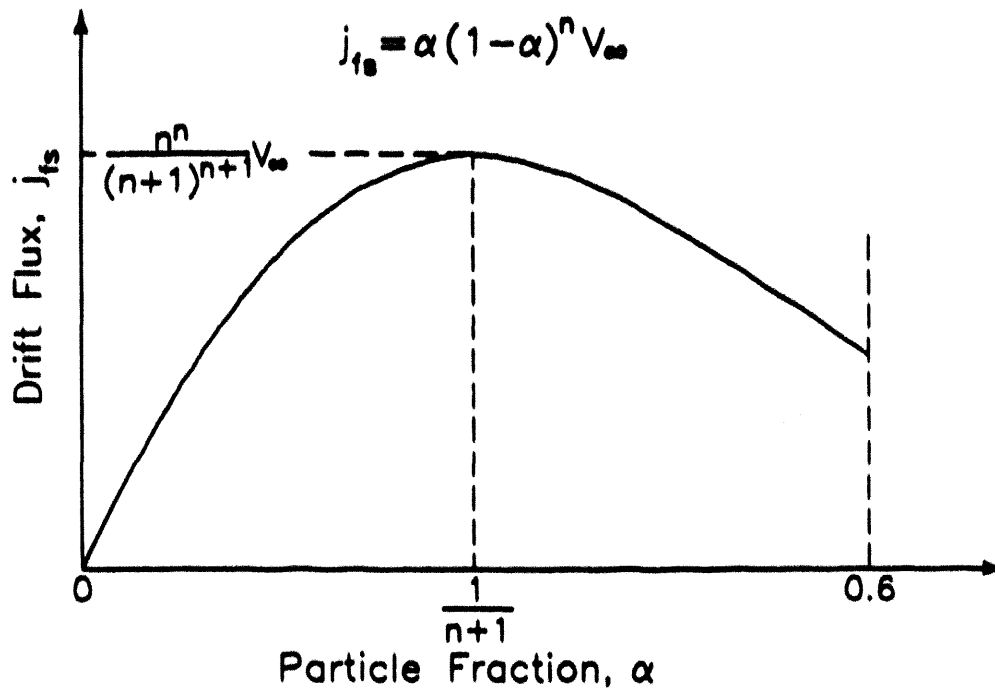


Figure 2: A Typical Curve of Drift-flux vs. Particle Fraction.

Wallis<sup>29</sup> has shown that the semi-empirical drift-flux model just described can be used to predict the dynamic behavior of a two-phase, two-component system under conditions of hindered settling. His analysis is based on the concept of continuity waves. In Section V, we will see that continuity waves arise as a consequence of the continuity equation.

## V. CONTINUITY WAVE METHOD

### A. General

The theory of continuity waves was first developed by Kynch.<sup>30</sup> He used this theory to predict the settling rate of particles during batch sedimentation under idealized conditions. The idealized conditions assume that the particle concentration is constant across any horizontal cross-section. Additional assumptions include identical particles of spherical shape which are large enough to prevent any tendency to flocculate. Shear stress at the vertical walls is also neglected. Batch sedimentation describes the settling behavior of an initially homogeneous mixture of particles, suspended in a fluid medium. The mixture is confined to a vessel of fixed volume and over time, the particles accumulate at the bottom of the vessel leaving a region of clear fluid above. This process is also referred to as hindered settling in some literature.

Experimental investigations have shown that three different settling modes are possible under conditions of hindered settling. The mode which will actually occur for a given system is dependent on the properties of the particles and the fluid. Kynch was able to use the theory of continuity waves to explain this phenomena. In Refs. 31, 32 and 33, Shannon, Tory and their co-workers have used the continuity wave method to analyze their experimental

results with good success. Additional details which distinguish the three modes of hindered settling are provided by Wallis in Ref. 29.

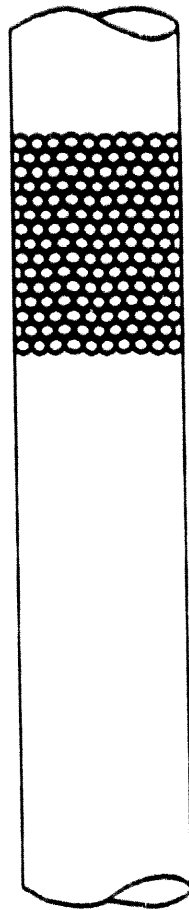
In this report, the application of continuity wave theory is extended to conditions of unrestrained settling. Unrestrained settling describes an initially homogeneous mixture of particles and fluid, below which there is a region of clear fluid. As the particles settle through the clear fluid, continuity wave theory predicts that a stable configuration of constant average velocity and constant particle fraction will be established. Figure 3 illustrates a simplified physical model of the unrestrained settling problem.

#### B. Continuity Wave Velocity

Continuity waves are best described as the propagation of continuous values of the particle fraction through a two-phase mixture. Propagation of the particle fraction in waves arises as a direct consequence of continuity requirements. In some literature, continuity waves are referred to as kinematic waves.

Consider the continuity equation for the particle phase, i.e. Eq. (17), expressed as:

$$\frac{\partial \alpha}{\partial t} + \frac{\partial}{\partial z}(\alpha v_s) = 0 \quad (65)$$



Close packing of identical spherical particles with diameter  $d$  are released from rest in a fluid-filled duct of diameter  $D \gg d$ .

Figure 3: A Simplified Physical Model of the Unrestrained Settling Problem.

Using the definition of the particle flux given in Eq. (57), we may re-write Eq. (65) as:

$$\frac{\partial a}{\partial t} + \frac{\partial}{\partial z} j_p = 0 \quad (66)$$

By assuming a condition of hydrodynamic equilibrium between the particle phase and the fluid phase, we may use the results of the steady-state analysis in Section IV to find

an expression for the particle flux. In view of Eq. (59), we obtain:

$$j_s = \alpha j + j_{s,r} \quad (67)$$

Substituting the expression for the particle drift-flux from Eq. (61) into Eq. (67), results in:

$$j_s = \alpha j \cdot \alpha(1 - \alpha) v_{rs} \quad (68)$$

Here, we see that the particle flux is a function of the particle fraction only. This observation was a crucial assumption in Kynch's development of the continuity wave theory.<sup>30</sup> Equation (68) shows that the validity of this assumption can be attributed to the invariance of the volumetric average velocity and the relative velocity between phases. We have established the invariance of  $j$  and  $v_{rs}$  with respect to the flow in Section IV. We are therefore justified in expressing the continuity relation of Eq. (66) as:

$$\frac{\partial \alpha}{\partial t} + \frac{\partial}{\partial \alpha} (j_s) \frac{\partial \alpha}{\partial z} = 0 \quad (69)$$

Since we know that the particle flux is independent of  $\partial \alpha / \partial t$  and  $\partial \alpha / \partial z$ , Eq. (69) is a first-order hyperbolic PDE of the following form:

$$\frac{\partial \alpha}{\partial t} + v_w \frac{\partial \alpha}{\partial z} = 0 \quad (70)$$

We recognize immediately that  $V_W$  in Eq. (70) is the velocity at which the dependent variable propagates in the  $z$ -direction. By comparison of Eqs. (69) and (70), we see that the continuity wave velocity is given by:

$$V_W = \frac{\partial}{\partial a} j, \quad (71)$$

Substituting the particle flux from the right-hand side of Eq. (67), we obtain:

$$V_W = j + \frac{\partial}{\partial a} j_{,r} \quad (72)$$

Time dependent problems involving particle motion are often formulated in terms of a diffusion process. When there are no source or sink terms, the diffusion equation can be written in the following general form:

$$\frac{Dn}{Dt} - \nabla \cdot \delta \nabla n = 0 \quad (73)$$

Here, we define:

- $n$  = number density of particles, #/cm<sup>3</sup>
- $\delta$  = particle diffusivity, cm<sup>2</sup>/s
- $\frac{D}{Dt}$  = substantial or material derivative

Multiplying Eq. (73) by the volume of a single particle, we obtain:

$$\frac{Dn}{Dt} - \nabla \cdot \delta \nabla n = 0 \quad (74)$$

In a one-dimensional Lagrangian coordinate system which moves at the volumetric average velocity  $j$ , Eq. (74) transforms to:

$$\frac{\partial a}{\partial t} + j \frac{\partial a}{\partial z} - \frac{\partial}{\partial z} \left( \delta \frac{\partial a}{\partial z} \right) = 0 \quad (75)$$

By substituting the continuity wave velocity from Eq. (72) into Eq. (70), we find that:

$$\frac{\partial a}{\partial t} + j \frac{\partial a}{\partial z} + \frac{\partial}{\partial a} (j_{,r}) \frac{\partial a}{\partial z} = 0 \quad (76)$$

Equation (76) can be re-written in a form which is similar to Eq. (75), namely:

$$\frac{\partial a}{\partial t} + j \frac{\partial a}{\partial z} + \frac{\partial}{\partial z} j_{,r} = 0 \quad (77)$$

In comparing this form with that of Eq. (75), we obtain the following relationship between the particle drift-flux, the diffusivity and the gradient of the particle fraction:

$$j_{,r} = - \delta \frac{\partial a}{\partial z} \quad (78)$$

We recognize the familiar form of Eq. (78) as Fick's law. The diffusivity could be determined from empirical measurements of the particle drift-flux and the gradient of the particle fraction.

When the diffusivity depends on the particle fraction, we see that Eq. (75) is a second-order non-linear PDE. Although Eq. (76) is also non-linear, it is only a first-order PDE. It appears that a formulation in terms of particle diffusion provides no particular advantage since Eq. (76) is easier to solve than Eq. (75). This point is

also discussed by Zuber and Staub in Ref. 34. Equation (76) is of the same form as Eq. (70) where the continuity wave velocity is given by Eq. (72). When the particle drift-flux for any condition of hydrodynamic equilibrium is determined by empirical methods, the continuity wave velocity is known and Eq. (70) will allow prediction of the transient response.

### C. Application to Unrestrained Settling

Unrestrained settling is defined as a homogeneous mixture of particles and fluid with a layer of clear fluid below. The particles are released from rest and settle through the region of clear fluid. Eventually, the particles attain a constant average velocity and a uniform particle fraction. Changes from the initial condition occur as a result of continuity waves which propagate through the mixture. When the hindered settling solution described by Wallis<sup>29</sup> is appended to the solution for unrestrained settling, the final motion of the particles is known and the solution is complete.

Consider the simplified model of unrestrained settling which is illustrated in Fig. 3. The particles are confined to a vertical duct of uniform cross-section. We will assume a value of 0.58 for the initial particle fraction. As the particles settle, a continuous state of hydrodynamic

equilibrium is maintained between the particle phase and the fluid phase. This hydrodynamic equilibrium is described by the semi-empirical drift-flux model of Eq. (62). Since the settling particles displace a volume of fluid which is equal to their own volume at each point in the flow, the net volumetric flux is zero. The continuity wave velocity from Eq. (72) therefore simplifies to:

$$V_w = \frac{\partial}{\partial \alpha} j_{sf} = - \frac{\partial}{\partial \alpha} j_{fs} \quad (79)$$

At a point of finite discontinuity in the particle fraction, an interface is clearly visible between two regions of different particle fractions. The movement of this interface is described as propagation of a shock wave. If the particle fraction in the upper region is designated  $\alpha_A$  and the particle fraction in the lower region is designated  $\alpha_B$ , then the shock wave velocity in the downward direction is given by:

$$V_{sAB} = \frac{(j_{fs})_A - (j_{fs})_B}{\alpha_A - \alpha_B} \quad (80)$$

In comparing Eqs. (79) and (80) to the graph of drift-flux vs. particle fraction (Fig. 2), we see that the continuity wave velocity is represented by the slope of a tangent line while the shock wave velocity is represented by the slope of a chord joining two points on the graph. At the point of maximum drift-flux, the slope of the

tangent line is zero and the continuity wave velocity vanishes. We will find that this point represents a stable condition of hydrodynamic equilibrium in which the average relative velocity between particles and fluid is maximized during unrestrained settling.

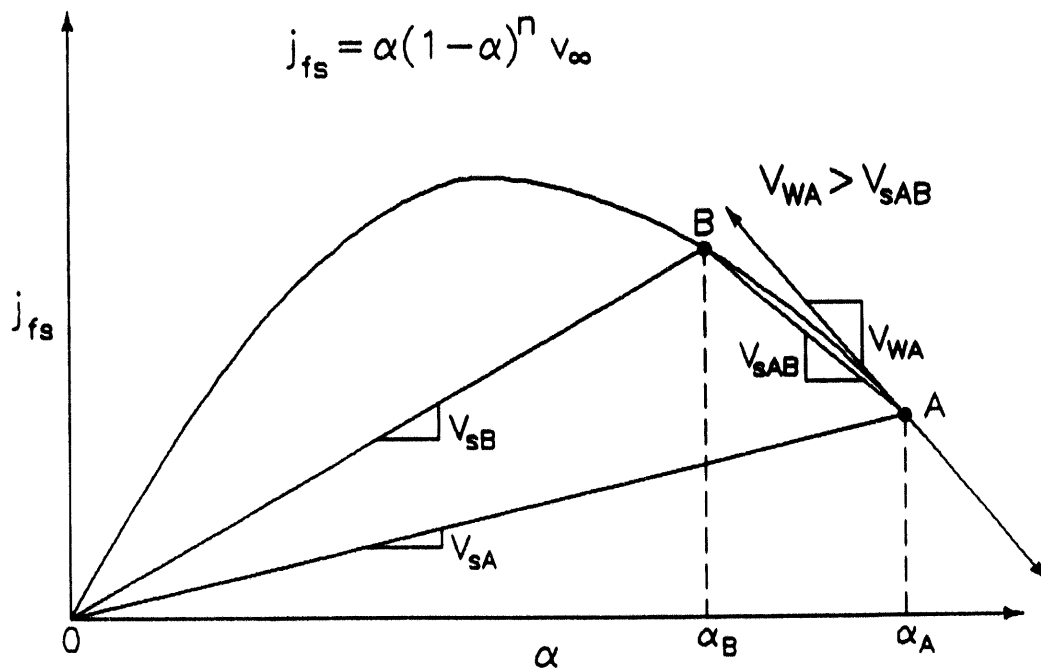


Figure 4: Drift-flux Curve Showing the Initial Settling Behavior. Note that the continuity wave velocity in region A exceeds the shock wave velocity between regions A and B.

After the particles in Fig. 3 are released from rest, they immediately begin to settle with a velocity given by the slope of the chord connecting  $\alpha_A$ ,  $(j_{fs})_A$  and  $\alpha = 0$ ,  $j_{fs} = 0$ , (see Fig. 4). Thus  $\alpha_A$  propagates downward with shock wave velocity  $V_{sA}$ :

$$V_{sA} = \frac{(j_{fs})_A - 0}{\alpha_A - 0} = (1 - \alpha_A)^n v_t \quad (81)$$

However, particles at the bottom will begin to settle faster because they are not restrained by particles below them. A region of lower particle fraction will therefore begin to form. Suppose that the particle fraction in this region is designated  $\alpha_B$  where  $\alpha_B < \alpha_A$ . The shock wave for region B causes  $\alpha_B$  to propagate downward with velocity  $V_{sB}$ :

$$V_{sB} = \frac{(j_{fs})_B - 0}{\alpha_B - 0} = (1 - \alpha_B)^n v_t > V_{sA} \quad (82)$$

Regions A and B are now separated by an interface at which  $\alpha_A$  changes abruptly to  $\alpha_B$ . This interface propagates downward with a velocity given by the slope of the chord joining  $\alpha_A$ ,  $(j_{fs})_A$  and  $\alpha_B$ ,  $(j_{fs})_B$ .

$$V_{sAB} = \frac{(j_{fs})_A - (j_{fs})_B}{\alpha_A - \alpha_B} = \left[ \frac{\alpha_A(1 - \alpha_A)^n - \alpha_B(1 - \alpha_B)^n}{\alpha_A - \alpha_B} \right] v_t \quad (83)$$

Recall that the continuity wave velocity in the downward direction is given by the slope of a line tangent to the curve of  $j_{fs}$ . Since  $j_{fs}$  is decreasing between  $\alpha_B$  and  $\alpha_A$ , the slope of the tangent line is negative and all

continuity waves in this region will propagate upward. Assume that the drift-flux curve is concave downward at all points, as shown in Fig. 4. In this case, at least some of the continuity waves will propagate faster than the shock wave  $V_{sAB}$ , represented by the interface between regions A and B. Shock wave  $V_{sAB}$  will therefore be reinforced resulting in a stable interface.

The argument in the preceding paragraph can be repeated until the drift-flux reaches its maximum value. When the drift-flux is maximized, there is maximum relative velocity between the particle phase and the fluid phase. The kinetic energy of the system is thus maximized while the potential energy decreases at a maximum rate. The maximum point on the  $j_{fs}$  curve occurs when the continuity wave velocity vanishes and represents a stable condition of hydrodynamic equilibrium. The particle fraction required to maximize the drift-flux is given by Eq. (63). The maximum drift-flux is given by Eq. (64). When these values are substituted into Eq. (82), we find that the maximum shock wave velocity in the downward direction is:

$$(V_{sB})_{\max} = \left[ \frac{n}{n+1} \right]^n v_t \quad (84)$$

After the shock wave  $V_{sAB}$  has propagated through the entire two-phase mixture, the average settling velocity of the particles will be given by Eq. (84) and the average

particle fraction of the homogeneous mixture will be given by Eq. (63).

If the cylindrical duct in the idealized settling problem of Fig. 3 is terminated in a solid bottom plate, the particles can be assumed to come to rest in inelastic collisions at the bottom. The final motion of the particles is described by the hindered settling problem analyzed by Wallis.<sup>29</sup> The final particle fraction is  $\alpha_A$  and the final drift-flux is zero. The shock wave between  $\alpha_A$  and  $\alpha_B$  propagates downward with velocity  $V_{sBA}$ , given by:

$$V_{sBA} = \frac{(j_{fs})_B - 0}{\alpha_B - \alpha_A} = \frac{\left[\frac{n}{n+1}\right]^n v_t}{\frac{1}{n+1} - 0.58} \quad (85)$$

The solution described by these results is easy to visualize by a plot in the  $z$ - $t$  plane. This plot represents a time history of the particle fraction vs. height. Figure 5 illustrates this solution for the case of a drift-flux curve which is concave downward at all points. Some typical numerical results are given in Table 4 for the case of boron-carbide particles in hot liquid sodium.

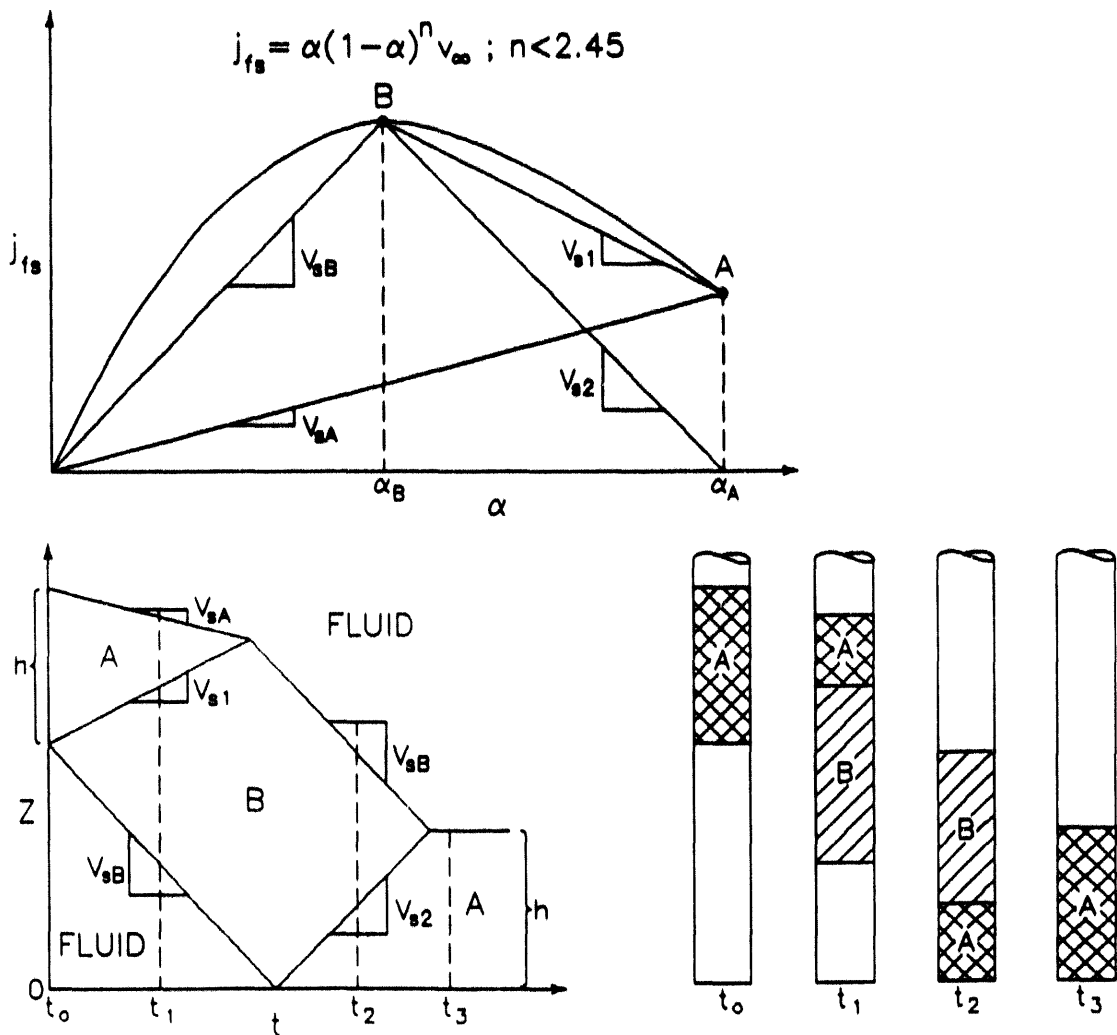


**Figure 5: A Time History of Multiple Particle Settling Behavior. Note the lack of an inflection point in the drift-flux curve.**

Table 4

Numerical Results for Particles with  $n < 2.45$ . These results are calculated for spherical boron-carbide particles in hot liquid sodium. They are based on the following numerical constants:  
 $\rho_s = 2510 \text{ kg/m}^3$ ;  $\rho_f = 883 \text{ kg/m}^3$ ;  $\mu = 3.45 \times 10^{-4} \text{ kg/(m-s)}$ ;  
 $g = 9.81 \text{ m/s}^2$ ;  $\sigma_A = 0.580$ . The designations for the shock wave velocities and the particle fractions refer to the illustration in Fig. 5. All velocities are expressed as positive in the downward direction.

d (cm)	d (in)	Re <sub>T</sub>	n	$\sigma_B$	v <sub>t</sub>	(cm/s)			
						V <sub>sA</sub>	V <sub>sB</sub>	V <sub>s1</sub>	V <sub>s2</sub>
0.635	0.250	9727	2.39	0.295	59.8	7.53	26.0	-11.3	-26.9
0.3175	0.125	3471	2.39	0.295	42.7	5.37	18.5	-8.24	-19.2
0.150	0.059	1033	2.39	0.295	26.0	3.39	11.7	-5.19	-12.1
0.120	0.047	714	2.39	0.295	23.2	2.92	10.1	-4.48	-10.4
0.090	0.035	438	2.42	0.292	19.0	2.32	8.23	-3.67	-8.35

When an inflection point occurs in the drift-flux curve, the solution is more complicated. An inflection point occurs when the second derivative of Eq. (62) vanishes. When the particle fraction at the point of inflection is less than the maximum particle fraction, the drift-flux curve will be concave upward to the left of  $\alpha_A$  in Fig. 4. This condition is only possible when the exponent  $n$  in the drift-flux model is greater than some limiting value, computed as follows:

$$\frac{2}{n+1} < 0.58$$

$$n > \frac{2 - 0.58}{0.58} = 2.45 \quad (86)$$

If the continuity wave velocity at  $\alpha_A$  is less than the shock wave velocity between  $\alpha_A$  and  $\alpha_B$ , a direct shock to  $\alpha_B$  is not possible. In this case, the time history of particle fraction vs. height is illustrated in Fig. 6. This figure shows that when the operating point in region B has moved far enough to the left, a shock wave will form between  $\alpha_B$  and  $\alpha_C$ . Region B represents a gradually decreasing particle fraction from  $\alpha_A$  to some lower limit where the shock wave to region C forms. Table 5 gives some typical numerical results for boron-carbide particles in hot liquid sodium which correspond to Fig. 6. Note that region B only forms when the continuity wave velocity at  $\alpha_A$  prevents the immediate formation of a shock wave.



**Table 5**

Numerical Results for Particles with  $n > 2.45$ . These results are calculated for spherical boron-carbide particles in hot liquid sodium. They are based on the following numerical constants:  
 $\rho_s = 2510 \text{ kg/m}^3$ ;  $\rho_f = 883 \text{ kg/m}^3$ ;  $\mu = 3.45 \times 10^{-4} \text{ kg/(m-s)}$ ;  
 $g = 9.81 \text{ m/s}^2$ ;  $\sigma_A = 0.580$ . The designations for the shock wave velocities, continuity wave velocities and particle fractions refer to the illustration in Fig. 6. All velocities are expressed as positive in the downward direction. Note that when the magnitude of the continuity wave velocity in region A ( $V_{WA}$ ) is less than the magnitude of the shock wave velocity between regions A and C ( $V_{S1}$ ), then a region of particle fraction  $\sigma_B$  does not form. In this case,  $\sigma_B = \sigma_A$ . However, region B forms immediately when the continuity wave velocity in region A prevents the formation of a direct shock wave to region C. When region B does form, it represents a region of continuous values of the particle fraction between  $\sigma_A = 0.580$  and the value of  $\sigma_B$  given in the table.

u  
u

d (cm)	d (in)	Re $\tau$	n	$\sigma_B$	$\sigma_C$	V $\tau$	(cm/s)				
							V $\sigma_A$	V $\sigma_C$	V $\sigma_A$	V $\sigma_C$	V $\sigma_1$
0.060	0.024	213	2.60	0.580	0.278	13.9	1.45	5.95	-3.76	-2.68	-5.45
0.030	0.012	55.0	2.98	0.580	0.251	7.16	0.540	3.02	-1.68	-1.36	-2.31
0.015	0.006	11.7	3.48	0.580	0.223	3.04	0.148	1.26	-0.565	-0.548	-0.789
0.0075	0.003	2.20	4.11	0.521	0.196	1.14	0.032	0.467	-0.151	-0.192	-0.238
0.0030	0.0012	0.174	4.58	0.480	0.179	0.227	0.004	0.092	-0.023	-0.037	-0.041

A third complication may arise when the drift-flux curve is extremely concave. This situation is illustrated in Fig. 7. In this figure, direct shock between  $\alpha_c$  and the fully packed state is not possible. As a result, region B reforms during the final stages of settling. This situation is the most complex process that can occur. The three cases considered here are analogous to the three modes of hindered settling described by Wallis.<sup>29</sup>

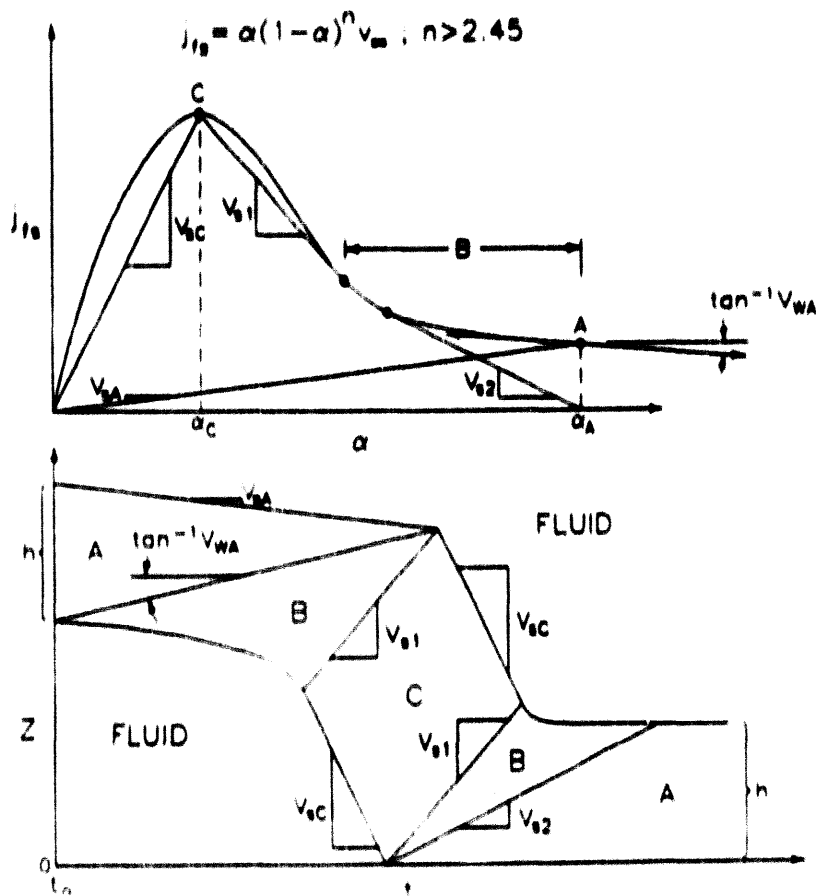


**Figure 7: A Time History of Multiple Particle Settling Illustrating the Re-formation of Region B During the Final Stages of Settling.**

## VI. CONCLUSIONS

We have seen that the velocity of a single particle in a quiescent liquid of infinite extent can be determined by solving an equation which considers the net sum of the forces acting on the particle. The solution indicates that the particle accelerates to 90% of its terminal velocity over a distance of about ten particle diameters. When the total distance of travel is much greater than ten particle diameters, the acceleration phase of the motion may be considered insignificant. When the particle is moving at its terminal velocity, it is in a condition of hydrodynamic equilibrium in which the weight of the particle in the liquid is just balanced by the drag force experienced by the particle.

We have also seen that when a mixture of particles and liquid is confined to a vertical duct of finite diameter, the particles attain a steady-state velocity which is less than the terminal velocity of a single particle. Each particle in the mixture experiences an increased drag force because the effective density and viscosity of the mixture are greater than those of the pure liquid. Conservation of momentum for the mixture and conservation of mass for each component are found to be insufficient conditions to determine the flow of a two-phase mixture. However, a closure relation can be obtained by writing a force balance

for a representative particle in the mixture. In this force balance, the transport properties are modified to account for both the presence of additional particles as well as their motion. This modification introduces the effective viscosity and an effective drag coefficient. When the modified transport properties are known, then the system of four differential equations has a deterministic solution.

From the steady-state solution for two-phase flow of a particle-fluid system, we found that the average relative velocity between the phases is an invariant parameter of the flow. This means that the relative velocity is independent of the average velocity of either component; an effect that has also been observed experimentally. The invariance of the volumetric average velocity when both phases are incompressible is established directly, by continuity considerations.

The volumetric average velocity may also be thought of as the net volumetric flux. The relative velocity between phases can be expressed in terms of the drift-flux. The drift-flux is the volumetric flux of either component with respect to a surface which moves at the volumetric average velocity. In the drift-flux model, the volumetric flux of particles is equal to the particle fraction times the net volumetric flux, plus the particle drift-flux. Since the

relative velocity is independent of the flow, the drift-flux can be empirically correlated by the expansion of a fluidized bed or the settling rates of suspensions. A graph of the drift-flux vs. particle fraction represents all points of hydrodynamic equilibrium between the particle and fluid phases. We have described such a correlation as a semi-empirical drift-flux model.

The continuity equation for the particle phase can also be expressed in terms of the volumetric flux of particles. Since the particle flux is dependent on the particle fraction only, the continuity equation has the form of a first-order hyperbolic PDE. This form suggests continuity waves which propagate at velocities corresponding to the derivative of the particle flux with respect to the particle fraction. If a condition of hydrodynamic equilibrium is maintained, then the semi-empirical drift-flux model can be introduced. With respect to the volumetric average velocity, the continuity wave velocity is the slope of a line tangent to the curve of drift-flux vs. particle fraction.

Although continuity wave theory has been applied to the problem of hindered settling, the unrestrained settling problem has not been previously addressed. Unrestrained settling has been defined as the settling behavior of a dense packing of particles which is released from rest in a

fluid-filled duct with a region of clear fluid below. Applications to backup shutdown systems for LMRs which use discreet absorber particles to provide the reactivity insertion, are expected to involve both types of settling. The initial settling behavior is modeled by the unrestrained settling problem and the final stages are modeled by the hindered settling problem.

We have shown that the method of continuity waves can be extended to predict unrestrained settling behavior when the semi-empirical drift-flux model is employed. The time dependent solution to the particle continuity equation is described in terms of continuity waves. The velocities of the continuity waves are predicted on the basis of a steady-state analysis which describes all conditions of hydrodynamic equilibrium in terms of the semi-empirical drift-flux model. At the point where the drift-flux is maximized, the continuity wave velocity vanishes and the continuity waves are unable to propagate. During conditions of unrestrained settling, this point represents a stable equilibrium in which the kinetic energy of the system is maximized and the potential energy is decreasing at a maximum rate.

When the hindered settling solution is appended to the unrestrained settling solution, the behavior of the multiple particle settling problem is completely described.

Three distinct modes of settling are possible. These modes are illustrated in Fig.'s 5, 6 and 7. These modes are easy to understand in terms of the shape of the drift-flux plot. The shape assumed by the drift-flux plot is determined by the physical properties of the fluid-particle system. Tables 4 and 5 present the results of numerical calculations for boron-carbide particles of various sizes in hot liquid sodium. Higher density absorber materials such as tantalum and tungsten are expected to provide faster continuity wave velocities than those obtainable with boron-carbide particles.

The results we have described are easily applied to specific systems which employ multiple particle settling. In a backup shutdown system for an LMR, the reactivity insertion as a function of time can be determined from the particle settling velocities predicted by this method. The significance of the analysis is that it ultimately enables the designer to predict the dynamic response of the core to shutdown transients.

Further work in this area should include experimental validation of the solution to the unrestrained settling problem. In addition, two-dimensional effects can be incorporated into the model. Such effects include expansion or constriction of the cross-sectional area normal to the flow and a non-uniform particle distribution

over the cross-section. Also, these results must be coupled to reactor kinetics calculations to demonstrate that backup shutdown systems which employ multiple particle settling are able to provide the required reactivity insertion rates and shutdown margins.

## REFERENCES

1. BEN JOSEPH SLIWINSKI; "Borated Microspheres for Emergency Shut-down of Light Water Nuclear Reactors", M.S. Thesis, University of Illinois, Urbana, IL (1983).
2. G. H. MILEY and R. W. BROCK; "Proposal for Development of a Final Shutdown Safety Rod for PRISM", Nuclear Engineering Report No. 315, University of Illinois, Urbana, IL (1990).
3. E. R. SPECHT, R. K. PASCHALL, M. MARQUETTE and A. JACKOLA; "Hydraulically Supported Absorber Balls Shutdown System for Inherently Safe LMFBR's", Proceedings of the International Meeting on Fast Reactor Safety and Related Physics, Vol. II, CONF-761001, pp. 683-695, Chicago, IL (Oct. 1976).
4. R. B. TUPPER and W. KWANT; "ALMR Reactivity Control and Shutdown System", Proceedings of the 1990 International Fast Reactor Safety Meeting, Vol. I, pp. 143-151, Snowbird, UT (Aug. 1990).
5. R. CLIFT, J. R. GRACE and M. E. WEBER; Bubbles, Drops and Particles, Academic Press, New York, NY (1978).
6. FAUT ODAR and W. S. HAMILTON; "Forces on a Sphere Accelerating in a Viscous Fluid", Journal of Fluid Mechanics, Vol. 18, pp. 302-314 (1964).
7. HANS RUMPF; Particle Technology, english edition translated by F. A. Bull, Chapman and Hall, New York, NY (1990).
8. S. L. SOO; Particulates and Continuum, Multiphase Fluid Dynamics, Hemisphere Publishing Corp. (1989).
9. N. ZUBER; "On the Dispersed Two-Phase Flow in the Laminar Regime", Chemical Engineering Science, Vol. 19, pp. 897-917 (1964).
10. A. EINSTEIN; "A New Determination of Molecular Dimensions", Annalen der Physik, Vol. 19(4), pp. 289-306 (1906). English translation appears in: Investigations on the Theory of the Brownian Movement by A. Einstein, Edited with notes by R. Furth, translated by A. S. Cowper, Dover Publications, Inc. (1956).

11. M. MOONEY; "The Viscosity of a Concentrated Suspension of Spherical Particles", Journal of Colloidal Science, Vol. 6, pp. 162-170 (1951).
12. VLADIMIR VAND; "Viscosity of Solutions and Suspensions, I", The Journal of Physical and Colloid Chemistry, Vol. 52, pp. 277-299 (1948).
13. VLADIMIR VAND; "Viscosity of Solutions and Suspensions, II", The Journal of Physical and Colloid Chemistry, Vol. 52, pp. 300-314 (1948).
14. H. C. BRINKMAN; "A Calculation of the Viscous Force Exerted by a Flowing Fluid on a Dense Swarm of Particles", Applied Scientific Research, Vol AI, pp. 27-34 (1949).
15. P. C. CARMAN; "Fluid Flow Through Granular Beds", Transactions of the Institution of Chemical Engineers, Vol. 15, pp. 150-166 (1937).
16. HAROLD H. STEINOUR; "Rate of Sedimentation, Nonflocculated Suspensions of Uniform Spheres", Industrial and Engineering Chemistry, Vol. 36(7), pp. 618-624 (1944).
17. D. R. OLIVER; "The Sedimentation of Suspensions of Closely-Sized Spherical Particles", Chemical Engineering Science, Vol. 15, pp. 230-242 (1961).
18. D. D. JOSEPH, A. F. FORTES, T. S. LUNDGREN and P. SINGH; "Nonlinear Mechanics of Fluidization of Spheres, Cylinders and Disks in Water", in Advances in Multiphase Flow and Related Problems, edited by George Papanicolaou, Society for Industrial and Applied Mathematics, Philadelphia, PA (1986).
19. J. F. RICHARDSON and W. N. ZAKI; "Sedimentation and Fluidisation: Part I", Transactions of the Institution of Chemical Engineers, Vol. 32, pp. 35-53 (1954).
20. J. F. RICHARDSON and R. A. MEIKLE; "Sedimentation and Fluidisation: Part III; The Sedimentation of Uniform Fine Particles and of Two-Component Mixtures of Solids", Transactions of the Institution of Chemical Engineers, Vol. 39, pp. 348-356 (1961).
21. JOHN GARSIDE and MAAN R. AL-DIBOUNI; "Velocity-Voidage Relationships for Fluidization and Sedimentation in Solid-Liquid Systems", Industrial and Engineering Chemistry, Process Design and Development, Vol. 16(2), pp. 206-214 (1977).

22. A. D. MAUDE and R. L. WHITMORE; "Generalized Theory of Sedimentation", British Journal of Applied Physics, Vol. 9, pp. 477-482 (1958).
23. K. E. BERTIL ANDERSSON; "Pressure Drop in Ideal Fluidization", Chemical Engineering Science, Vol. 15, pp. 276-297 (1961).
24. FLUIDIZATION; second edition, edited by; J. F. Davidson, R. Clift and D. Harrison, Academic Press, Orlando, FL (1985).
25. LEON LAPIDUS and J. C. ELGIN; "Mechanics of Vertical-moving Fluidized Systems", American Institute of Chemical Engineers' Journal, Vol. 3(1), pp. 63-68 (1957).
26. B. G. PRICE, L. LAPIDUS, and J. C. ELGIN; "Mechanics of Vertical Moving Fluidized Systems: II. Application to Countercurrent Operation", American Institute of Chemical Engineers' Journal, Vol. 5(1), pp. 93-97 (1959).
27. J. A. QUINN, LEON LAPIDUS; and J. C. ELGIN; "The Mechanics of Moving Vertical Fluidized Systems: V. Concurrent Cogravity Flow", American Institute of Chemical Engineers' Journal, Vol. 7(2), pp. 260-263 (1961).
28. A. G. BRIDGE, LEON LAPIDUS, and J. C. ELGIN; "The Mechanics of Vertical Gas-Liquid Fluidized Systems: I. Countercurrent Flow", American Institute of Chemical Engineers' Journal, Vol. 10(6), pp. 819-826 (1964).
29. GRAHAM B. WALLIS; One Dimensional Two-Phase Flow, McGraw-Hill Inc. (1969).
30. G. J. KYNCH; "A Theory of Sedimentation", Transactions of the Faraday Society, Vol. 48(2), pp. 166-176 (1952).
31. PAUL T. SHANNON, ELWOOD STROUPE, and ELMER M. TORY; "Batch and Continuous Thickening; Basic Theory: Solids Flux for Rigid Spheres", Industrial and Engineering Chemistry, Fundamentals, Vol. 2(3), pp. 203-211 (1963).
32. PAUL T. SHANNON, ROBERT D. DEHAAS, ELWOOD P. STROUPE, and ELMER M. TORY; "Batch and Continuous Thickening; Prediction of Batch Settling Behavior from Initial Rate Data with Results for Rigid Spheres", Industrial and Engineering Chemistry, Fundamentals, Vol. 3(3), pp. 250-260 (1964).

33. P. T. SHANNON and E. M. TORY; "Settling of Slurries; New Light on an Old Operation", Industrial and Engineering Chemistry, Vol. 57(2), pp. 18-25 (1965).
34. NOVAK ZUBER and F. W. STAUB; "The Propagation and the Wave Form of the Vapor Volumetric Concentration in Boiling, Forced Convection System Under Oscillatory Conditions", International Journal of Heat Transfer, Vol. 9, pp. 871-895 (1966).

**DATE  
FILMED**

12 / 7 / 93

**END**

